Inorganic Chemistry

Article

pubs.acs.org/IC

$NaCu_6Se_4$: A Layered Compound with Mixed Valency and Metallic Properties

Mihai Sturza,[†] Christos D. Malliakas,[†,‡] Daniel E. Bugaris,[†] Fei Han,[†] Duck Young Chung,[†] and Mercouri G. Kanatzidis*[,†,‡]

[†]Materials Science Division, Argonne National Laboratory, 9700 South Cass Avenue, Argonne, Illinois 60439, United States

[‡]Department of Chemistry, Northwestern University, 2145 Sheridan Road, Evanston, Illinois 60208, United States

Supporting Information

ABSTRACT: A new ternary compound $NaCu_6Se_4$ was synthesized from the reaction of Cu in a molten sodium polyselenide flux. The compound crystallizes in trigonal space group $R\bar{3}m$ with a = 4.0465(3) Å and c = 41.493(5) Å. The crystal structure contains flat two-dimensional slabs of $^1/_\infty[Cu_6Se_4]$ with a unique structural arrangement, separated by Na cations. The compound contains mixed valency and has a high conductivity of ~3 × 10^3 S cm^{-1} at room temperature, and exhibits increasing conductivity with decreasing temperature, indicating metallic behavior. A small positive thermopower (4−11 μV K^{-1} from 300 to 500 K) and Hall effect measurements indicate p-type transport with a carrier concentration of ~2.8(3) × 10^{21} cm^{-3} and a hole mobility of ~8.75 cm^2 V^{-1} s^{-1} at 300 K. $NaCu_6Se_4$ exhibits temperature-independent Pauli paramagnetism.

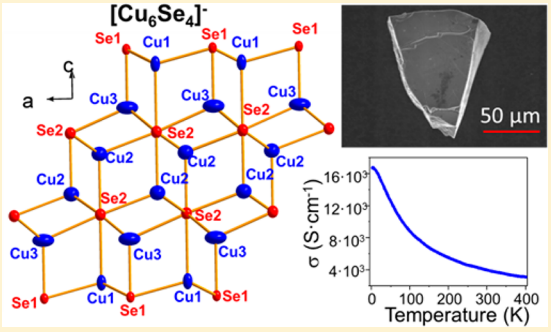

INTRODUCTION

Copper chalcogenide materials are of considerable scientific interest because of their rich structural and compositional diversity,[1,2] mixed valency,[3,4] propensity for phase transitions,[5−7] potential for ionic mobility,[8,9] as well as applications such as high performance photovoltaic cells.[10] The structural dimensionality of ternary A/Cu/Q compounds (A = alkali, Q = S, Se, Te) is generally affected by the alkali cations.[11,12] Ternary copper chalcogenides can be categorized into those which are valence-precise containing Cu^+ and Q^{2-}, and those which require a mixed valence Cu^+/Cu^{2+} formalism to be properly described. Determining the oxidation state of copper in chalcogenides is challenging due to the high covalency of the Cu−Q bonds and the similar energies of Cu d and Q p orbital states. The consensus is that mixed valency is generated by the chalcogen sublattice, rather than Cu itself, where the chalcogen can achieve −2/−1 mixed valency.[13] However, Cu definitely plays a key role by participating in the mixed valency contributing +1/+2 pairs since other metals such as Ag, Au, Zn, etc. do not form compounds in which the chalcogen achieves −2/−1 states. It is best if we think of these compounds as simply mixed-valent where the ground state is defined by a linear combination of $S^{2-/1-}$ and $Cu^{1+/2+}$ states. Thus, valence-precise copper chalcogenides behave as semiconductors, whereas mixed-valent copper chalcogenides display p-type metallic conductivity. Particularly, these mixed-valent Cu chalcogenides feature a broad array of structures including the following: mono-dimensional networks (1D) in $Na_3Cu_4S_4$,[3,4] two-dimensional (2D) networks in $NaCu_4S_4$,[14] ACu_4Q_3 (A = K, Rb, Cs, Tl; Q = S, Se),[15] $A_3Cu_8Q_6$ (A = K, Rb, Cs; Q = S, Se),[16−18] $A_3Cu_8Te_{10}$ (A = Rb, Cs),[19] $Cs_2Cu_5Se_4$,[20] $TlCu_2Q_2$ (Q = S, Se),[21] $TlCu_6S_4$,[22] $Tl_5Cu_{14}Se_{10}$,[23] and three-dimensional (3D) networks, such as $K_4Cu_8Te_{11}$,[19] $K_3Cu_{11}Te_{16}$,[24] $K_2Cu_5Te_5$,[25] and $Cs_3Cu_{20}Te_{13}$.[26]

Since the discovery of high-temperature superconductivity in mixed-valent Cu oxides, such as YBCO (yttrium barium copper oxide) and LSCO ($La_{2-x}Sr_xCuO_4$, lanthanum strontium copper oxide), the related oxide compounds have been extensively studied. The corresponding mixed-valent Cu chalcogenides have also been of significant interest because they too exhibit metallic conductivity,[19,29] superconductivity,[28−30] phase transitions,[31,32] and charge-density waves.[33]

Here we report new results from the chemistry of the Na/Cu/Se system in which NaCuSe is the only reported phase.[34] We began this investigation in an effort to study the selenide analogue of the mixed-valent $NaCu_4S_4$ compound. Instead, we discovered a new compound that features a unique 2D structure. We report the synthesis, structure, and properties of $NaCu_6Se_4$, which is mixed-valent and p-type metallic. Density functional theory (DFT) calculations explain the origin of holes in the metallic 2-D framework and agree well with the experimental results of Pauli paramagnetism and the temperature trend of the electrical conductivity.

EXPERIMENTAL SECTION

Synthesis of $NaCu_6Se_4$. The following reagents were used as received: sodium selenide (99.9%, Sigma-Aldrich), selenium (99.999%,

Received: September 4, 2014
Published: October 31, 2014

   dx.doi.org/10.1021/ic502137m | Inorg. Chem. 2014, 53, 12191−12198

Spectrum Chemical Mfg. Corp.), copper (99.9%, Sigma-Aldrich), and sodium (99.9%, Sigma-Aldrich). The phase-pure binary compounds CuSe and Cu_2Se were prepared from the elements by heating at a temperature of 600 °C for 72 h.

All chemical handling was carried out in a glovebox under a dry argon atmosphere. In this exploration of the Na/Cu/Se system, we initially attempted the synthesis procedure reported[14] for $NaCu_4S_4$. A 12 mm diameter fused-silica tube containing Cu (0.032 g, 0.5 mmol), Na_2Se (0.187 g, 1.5 mmol), and Se powder (0.236 g, 3 mmol) was evacuated and flame-sealed under a pressure of $<10^{-4}$ mbar. The tube was heated at 600 °C for 48 h and then cooled slowly at a rate of 6 °C/h to 50 °C. Excess polyselenide flux was removed by washing the product with *N*,*N*′-dimethylformamide and methanol. Unlike the sulfur system, two kinds of crystals were obtained: dark blue trigonal plate crystals of $NaCu_6Se_4$ (~75% yield) and black thin plate crystals of NaCuSe (~25% yield).

Once the stoichiometry of $NaCu_6Se_4$ was determined from the refinement of single-crystal X-ray structural data, it was directly synthesized as a pure phase in quantitative yield by two different synthetic routes.

Method A. A stoichiometric mixture of CuSe (0.285 g, 2 mmol), Cu_2Se (0.412 g, 2 mmol), and Na (0.023 g, 1 mmol) was loaded in an alumina crucible covered with an alumina cap and flame-sealed inside a fused-silica tube under a pressure of $<10^{-4}$ mbar. The tube was heated to 600 °C in 20 h, soaked at that temperature for 24 h, and subsequently cooled at a rate of 50 °C/h to room temperature. The partially reacted mixture was then homogenized by grinding in a mortar to a fine dark blue powder. The powder was then reannealed at 400 °C for 5 days and quenched to room temperature.

Method B. $NaCu_6Se_4$ was also prepared by a stoichiometric reaction of the elements. A mixture of 0.023 g (1 mmol) Na, 0.381 g (6 mmol) Cu, and 0.316 g (4 mmol) Se was loaded in an alumina crucible, closed with an alumina cap, and then flame-sealed under vacuum ($<10^{-4}$ mbar) inside a fused-silica tube. The mixture was slowly heated to form a complete melt at 600 °C and kept there for 6 h, followed by cooling to room temperature in 6 h. The resulting mixture was then homogenized by grinding with a mortar and pestle to a fine dark blue powder. To obtain pure polycrystalline $NaCu_6Se_4$, the homogenized mixture was annealed at 400 °C for 7 days and then quenched to room temperature. Purity of the air-stable products from these two methods was checked by powder X-ray diffraction (XRD) and energy-dispersive X-ray spectroscopy (EDS).

Single-Crystal X-ray Diffraction. A thin trigonal plate single crystal of $NaCu_6Se_4$ was selected and mounted on the tip of a glass fiber for X-ray diffraction. Intensity data were collected at room temperature using ω scans on a STOE imaging plate diffraction system (IPDS-II) using graphite-monochromatized Mo Kα radiation (λ = 0.710 73 Å) operating at 50 kV and 40 mA with a 34 cm diameter imaging plate. Individual frames were collected with a 3 min exposure time and a 1° ω rotation. X-AREA, X-RED, and X-SHAPE software packages[35] were used for data collection, integration, and analytical absorption corrections, respectively. SHELXL[36] and JANA2006[37] software packages were used to solve and refine the structure. The parameters for data collection and the details of the structure refinement are given in Table 1. Atomic coordinates, thermal displacement parameters (U_{eq}), and occupancies of all atoms are given in Table 2. Anisotropic displacement parameters and selected bond lengths and angles are given in Tables 3 and 4.

Powder X-ray Diffraction and Scanning Electron Microscopy. Phase purity of the products was assessed by powder XRD. The products were finely ground and mounted on a flat plate sample holder. Diffraction data were collected on a Panalytical X'pert Pro diffractometer with an iron-filtered Cu Kα source, operating at 45 kV and 40 mA under a continuous scanning method in the 2θ range 5–120° with a step size of 0.0167°. Powder XRD data were analyzed with the Rietveld method using the FULLPROF 2000 program.[38] The background was fitted using linear interpolation between selected points. The March–Dollase model for preferred orientation was used in all of the refinements, and a pseudo-Voigt function was used as the peak-shape model. The refinement includes anisotropic displacement parameters (ADPs) for individual atoms.

Semiquantitative microprobe analysis of several crystals was performed with a Hitachi S-4700-II scanning electron microscope equipped with an EDAX Phoenix X-ray energy dispersive spectrometer (EDS). The spectrometer utilizes a Li-drifted Si detector with an ultrathin window, and data were acquired with a beam current of 10

Table 1. Summary of Crystallographic Data and Structure Refinement for $NaCu_6Se_4$ at 293 K

empirical formula	$NaCu_6Se_4$
fw	720.1
T	293(2) K
wavelength	0.710 69 Å
crystal system	trigonal
space group	$R\bar{3}m$
unit cell dimensions	$a = b$ = 4.0465(3) Å, c = 41.493(5) Å
V	588.39(9) Å^3
Z	3
density (calcd)	6.0948 g/cm^3
abs coeff	34.485 mm^{-1}
F(000)	934
crystal size	0.0236 × 0.0158 × 0.0058 mm^3
θ range for data collection	4.42–24.95°
index ranges	$-4 \le h \le 4$; $-4 \le k \le 4$; $-48 \le l \le 43$
reflns collected	1276
indep reflns	174 [R_{int} = 0.0866]
completeness to θ = 24.95°	98.9%
refinement method	full-matrix least-squares on F^2
data/restraints/params	174/0/18
GOF	1.147
final R indices [$>2\sigma(I)$][a]	R_{obs} = 0.0616, wR_{obs} = 0.1539
R indices [all data][a]	R_{all} = 0.0651, wR_{all} = 0.1563
largest diff peak and hole	2.472 and −2.024 e Å^{-3}

[a] $R = \Sigma||F_o| - |F_c||/\Sigma|F_o|$, $wR = \{\Sigma[w(|F_o|^2 - |F_c|^2)^2]/\Sigma[w(|F_o|^4)]\}^{1/2}$ and $w = 1/(\sigma^2(F) + 0.0001F^2)$.

Table 2. Atomic Coordinates (×10^4) and Equivalent Isotropic Displacement Parameters (Å^2 × 10^3) of $NaCu_6Se_4$ at 293(2) K

atom	Wyckoff	x	y	z	occupancy	U_{eq}[a]
Na(1)	3*b*	3333	6667	1667	1	22(7)
Cu(1)	6*c*	−3333	3333	1064(2)	1	25(2)
Cu(2)	6*c*	3333	6667	195(2)	1	41(2)
Cu(3)	6*c*	0	0	642(2)	1	66(3)
Se(1)	6*c*	0	0	1211(1)	1	15(1)
Se(2)	6*c*	6667	3333	400(1)	1	22(2)

[a] U_{eq} is defined as one-third of the trace of the orthogonalized U_{ij} tensor.

Table 3. Anisotropic Displacement Parameters (Å^2 × 10^3) for $NaCu_6Se_4$ at 293(2) K[a]

atom	U_{11}	U_{22}	U_{33}	U_{12}	U_{13}	U_{23}
Na(1)	22(8)	22(8)	21(11)	11(4)	0	0
Cu(1)	16(2)	16(2)	43(3)	8(1)	0	0
Cu(2)	43(3)	43(3)	36(3)	22(2)	0	0
Cu(3)	84(4)	84(4)	29(3)	42(2)	0	0
Se(1)	12(2)	12(2)	21(2)	6(1)	0	0
Se(2)	21(2)	21(2)	24(2)	10(1)	0	0

[a] The anisotropic displacement factor exponent takes the form $-2\pi^2[h^2a^{*2}U_{11} + \ldots + 2hka^*b^*U_{12}]$.

dx.doi.org/10.1021/ic502137m | *Inorg. Chem.* 2014, 53, 12191–12198

Table 4. Representative Bond Lengths (Å) and Bond Angles (deg) of $NaCu_6Se_4$ at 293(2) K

atom−atom	bond lengths	atom−atom−atom	bond angle
Cu(1)−Se(1) (×3)	2.414(4)	Se(1)−Cu(1)−Se(1)	113.85(1)
Cu(1)−Se(2) (×1)	2.755(6)	Se(1)−Cu(1)−Se(2)	104.62(2)
Cu(2)−Se(2) (×1)	2.467(6)	Se(2)−Cu(2)−Se(2)	108.91(4)
Cu(2)−Se(2) (×3)	2.487(2)	Se(2)−Cu(2)−Se(2)	110.03(4)
Cu(3)−Se(1) (×1)	2.362(6)	Se(1)−Cu(3)−Se(2)	113.23(3)
Cu(3)−Se(2) (×3)	2.542(3)	Se(2)−Cu(3)−Se(2)	105.46(5)
Na(1)−Se(1) (×6)	3.006(8)	Cu(3)−Se(2)−Cu(1)	66.77(3)
Na(1)−Cu(1) (×6)	3.423(3)	Cu(2)−Se(2)−Cu(1)	110.03(4)
Cu(1)−Cu(3) (×3)	2.920(5)	Se(1)−Na(1)−Se(1)	180
Cu(2)−Cu(2) (×3)	2.840(6)	Se(1)−Na(1)−Cu(1)	94.05(7)
Cu(2)−Cu(3) (×3)	2.983(5)	Cu(1)−Na(1)−Cu(1)	180

μA at 20 kV accelerating potential. Analysis on several crystals indicates an average composition of $Na_{0.9(1)}Cu_{5.8(2)}Se_{3.9(2)}$, which is in good agreement with the composition obtained from the single-crystal X-ray structure refinement.

Differential Thermal Analysis. Differential thermal analyses (DTA) were carried out with a Shimadzu DTA-50 thermal analyzer. The ground sample (~60 mg total mass) was sealed in a carbon-coated fused-silica ampule under vacuum. A fused-silica ampule containing alumina of equal mass was sealed and used as a reference. The sample was heated to 550 °C at 5 °C/min, followed by cooling at the same rate to 50 °C. The stability of the sample and reproducibility of the measurement were monitored by running multiple heating and cooling cycles. Residues of the DTA experiments were examined with powder X-ray diffraction.

Charge Transport and Magnetic Properties. Variable-temperature four-probe resistivity and Hall effect measurements on annealed, pressed pellets of $NaCu_6Se_4$ were performed with a Quantum Design PPMS. The annealing of the pellets was done at 400 °C for 3 days, followed by quenching to room temperature. The temperature range was 2−400 K for resistivity and 2−300 K for Hall effect measurement. The Hall effect was measured by reversing the magnetic field $H = \pm 9$ T. Measurements were performed in four-probe geometry with 30 μm gold wires and silver paste used for the current and voltage electrodes, respectively. Resistivity measurements were conducted using a homemade apparatus equipped with a nanovoltmeter (Keithley 2182A), an electrometer (Keithley 6514), and a high-temperature vacuum chamber governed by a temperature controller (MMR Technologies K-20). For the Seebeck coefficient measurement, a pressed pellet of $NaCu_6Se_4$ was mounted on the stage and attached to the thermocouples with colloidal silver liquid. The measurement was performed in the temperature range 300−450 K, above which the silver paste would react with the sample. The Seebeck voltage $V(T)$ was measured by the integral method, in which one end of the sample is held at a fixed temperature T_0, and the other end is varied through the temperature T range of interest using a commercial MMR Technologies SB-100 Seebeck measurement system. The Seebeck coefficient S is obtained from the slope of the $V(T)$ versus T curve, i.e., $S = dV(T)/dT$.[39]

Magnetic susceptibility measurements were carried out with a Quantum Design MPMS-XL SQUID magnetometer. Polycrystalline powder of $NaCu_6Se_4$ was loaded in a gelatin capsule. Corrections for the diamagnetism of the PVC sample container and the diamagnetism of the atoms were applied. Temperature-dependent data were collected under zero-field-cooled (ZFC) and field-cooled (FC) conditions between 2 and 300 K, with an applied field $H = 0.5$ T. The experimental data were fitted against a modified Curie−Weiss law $[\chi = \chi_0 + C/(T - \theta)]$, where χ is the molar magnetic susceptibility, χ_0 is the temperature-independent paramagnetic susceptibility, C is the Curie constant, and θ is the Curie temperature.

Band Structure Calculations. Electronic structure calculations were performed using the self-consistent full-potential linearized augmented plane wave method (LAPW)[40] within density functional theory (DFT),[41,42] and the generalized gradient approximation (GGA) of Perdew, Burke, and Ernzerhof[43] for the exchange and correlation potential. The values of the atomic radii were taken to be 2.2 au for Se atoms, 2.24 au for Cu atoms, and 2.5 au for Na atoms, where au is the atomic unit (0.529 Å). Convergence of the self-consistent iterations was performed for 891 k points inside the irreducible Brillouin zone to within 0.0001 Ry with a cutoff of −6.0 Ry between the valence and the core states. Scalar relativistic corrections were included, and a spin−orbit interaction was incorporated using a second variational procedure.[44] The calculations were performed using the WIEN2k program using the experimentally obtained cell constants and atomic coordinates.[45]

RESULTS AND DISCUSSION

Synthesis. The single crystals of $NaCu_6Se_4$ were first observed in the product of the reaction of Cu in molten sodium polyselenide. Excess polyselenide flux could be removed by washing with *N*,*N*′-dimethylformamide and methanol, leaving behind thin plate-like dark blue crystals of $NaCu_6Se_4$ (~75% yield) and thin black plate crystals of NaCuSe (~25% yield). After multiple attempts to optimize the synthetic condition for $NaCu_6Se_4$, the two-step reaction of a stoichiometric combination of binary CuSe and Cu_2Se with Na or elemental mixture was found to produce a pure single phase of target compound: (1) prereaction at 600 °C and homogeneous mixing by grinding, and (2) long time annealing at a low temperature and quenching. The single phase of $NaCu_6Se_4$ was confirmed by Rietveld refinement of the powder X-ray diffraction data (Figure 1). The results are in good agreement (Bragg R = 5.60%, R_f-factor = 8.09%) with the structural parameters determined from the single-crystal X-ray diffraction.

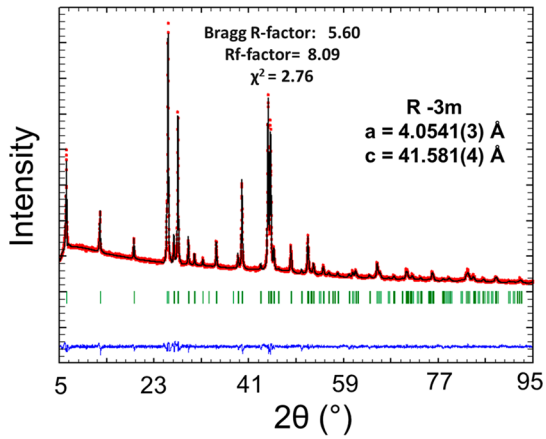

Figure 1. Calculated and observed XRD patterns of the Rietveld refinement for $NaCu_6Se_4$ (λ = 1.5406 Å, Bragg R-factor: 5.60%; R_f-factor = 8.09%; Bragg R-factor = $\Sigma|I_{ko} - I_{kc}|/\Sigma I_{ko}$; R_f-factor = $[(N - P)/\Sigma w_i \cdot y_{io}^2]^{1/2}$).

Differential thermal analysis (DTA) on polycrystalline $NaCu_6Se_4$ with heating at a rate of 5 °C/min to a maximum temperature of 550 °C showed an endothermic melting peak at approximately 490 °C, as well as a related exothermic crystallization around 475 °C (Figure 2a). Over continuous heating, a second endothermic melting peak around 515 °C and the related exothermic peak around 500 °C appeared, and can be related to an unidentified phase that forms in heating by decomposition of the $NaCu_6Se_4$ phase. After multiple cycles of heating−cooling, the resulting sample was investigated by

dx.doi.org/10.1021/ic502137m | Inorg. Chem. 2014, 53, 12191−12198

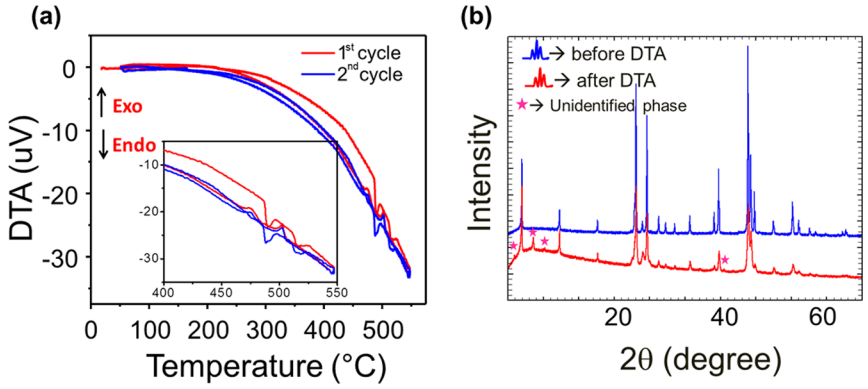

Figure 2. (a) Differential thermal analysis (DTA) of $NaCu_6Se_4$ showing a melting and crystallization event (experiment run under vacuum; heating/cooling rate 5 °C/min). (b) X-ray powder diffraction patterns observed from a sample of $NaCu_6Se_4$ after a DTA experiment run at 550 °C showing the appearance of an extra phase and noncongruent melting.

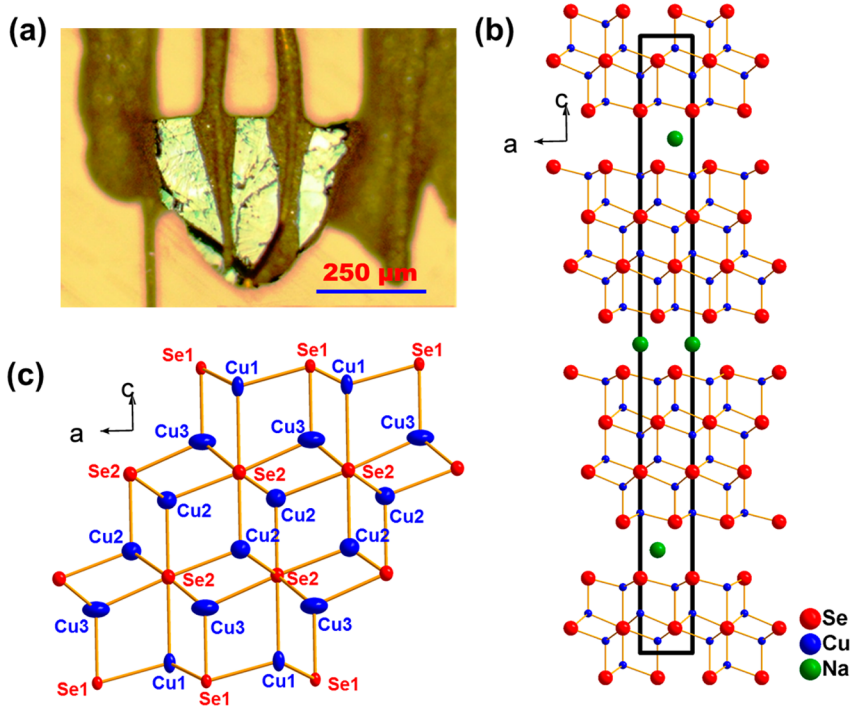

Figure 3. (a) Optical image of a typical $NaCu_6Se_4$ crystal. (b) Perspective view of the layered structure of $NaCu_6Se_4$ viewed down the crystallographic *b* axis. (c) Projection of $[Cu_6Se_4]$ layer viewed along the *b*-axis direction with thermal ellipsoids set at 50%. Na atoms are green, Cu atoms are blue, and Se atoms are red.

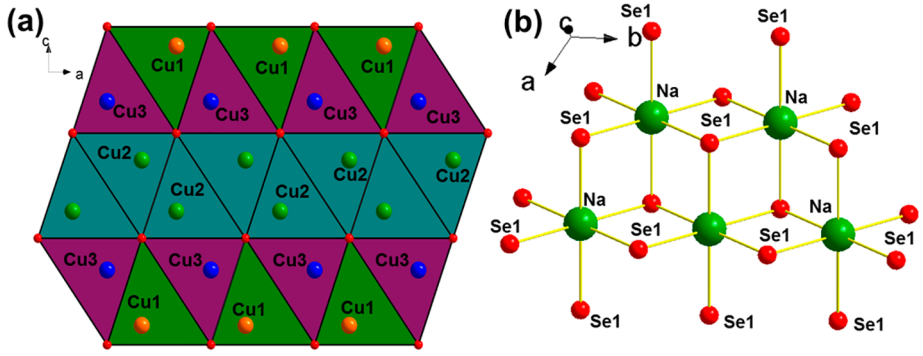

Figure 4. (a) Polyhedral representation of $[Cu_6Se_4]$ layer viewed along the *b*-axis direction. (b) Local coordination environment of Na.

powder X-ray diffraction, which revealed an unidentified phase, suggesting $NaCu_6Se_4$ melts incongruently (Figure 2b).

Crystal Structure. The crystal structure of $NaCu_6Se_4$ was determined from single-crystal X-ray diffraction data collected

dx.doi.org/10.1021/ic502137m | *Inorg. Chem.* 2014, 53, 12191−12198

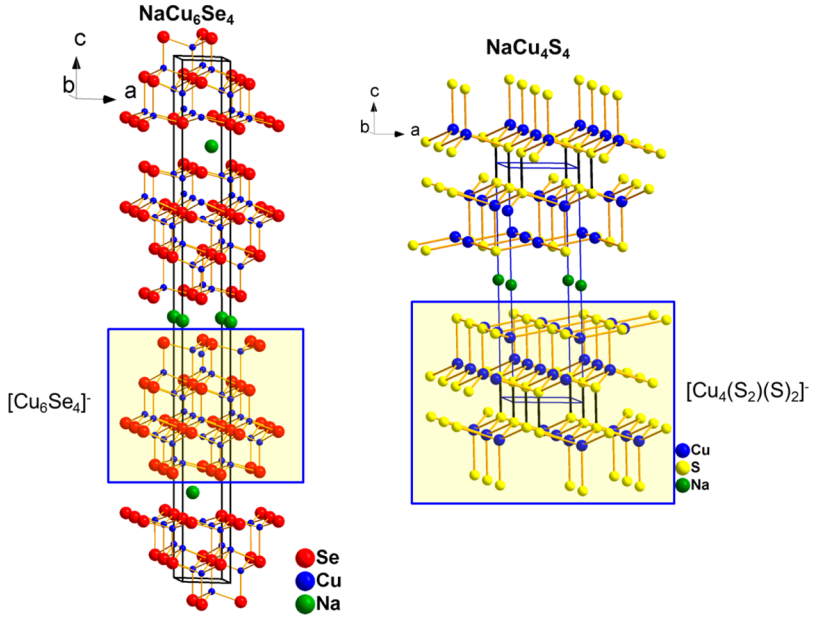

Figure 5. Comparative view of the layered structures of $NaCu_6Se_4$ and $NaCu_4S_4$ viewed along the crystallographic *b* axis. Na atoms are green, Cu atoms are blue, Se atoms are red, and S atoms are yellow.

at room temperature. The crystallographic data and selected bond distances and bond angles for $NaCu_6Se_4$ are listed in Tables 1−4. The dark blue plate crystal of $NaCu_6Se_4$, depicted in Figure 3a, crystallizes in the rhombohedral space group $R\bar{3}m$, with cell parameters of a = 4.0465(3) Å, c = 41.493(5) Å, and Z = 3. The structure of $NaCu_6Se_4$ consists of a unique two-dimensional network of $[Cu_3Se_2]$ layers, which are separated by the Na cations (Figure 3b).

The structure of the $[Cu_6Se_4]^-$ slab is composed of tetrahedral Cu centers that share edges to form layers in the *ab* plane (Figure 3c). Three crystallographically distinct Cu atoms are located in each layer. The view of copper polyhedra in the $[Cu_6Se_4]^-$ slabs along the crystallographic *b* axis is depicted in Figure 4a. Cu(1) is tetrahedrally coordinated by three Se(1) and one Se(2), Cu(2) by four Se(2), and Cu(3) by one Se(1) and three Se(2). The Cu−Se distances for Cu(1) are 2.414(4) and 2.755(6) Å, for Cu(2) it is 2.477(6) Å, and for Cu(3) they are 2.362(6) and 2.542(3) Å. The bonding angles around Cu and Se are consistent with a distorted tetrahedral geometry. All the Cu−Se distances and angles compare favorably with those found in other copper selenides, including NaCuSe,[34] $Cu_{2-x}Se$,[46] CuSe,[47] and Cu_3Se_2.[48] The coordination environment of Na is shown in Figure 4b. Na^+ cations are located between the $[Cu_6Se_4]^-$ slabs, with an octahedral arrangement of Se atoms, with Na···Se distances of 3.0061(8) Å. During the structure refinement, we observed large anisotropic displacement parameters for the atoms Cu(3) at room temperature. The largest value is obtained for U_{11} and U_{22}. The refinement of the occupancy of the Cu(3) in the distorted tetrahedral environment does not fix this problem. Large ADPs in this class of compounds are indicative of dynamic or static disorder, which is due to the high thermal motion of the Cu ions. We note that similar results were reported for $A_3Cu_8Q_6$ (A = K, Rb, Cs; Q = S, Se).[16−18]

The crystal structure of $NaCu_6Se_4$ can be compared with a 2D metallic chalcogenide compound $NaCu_4S_4$,[14] built by anionic $[Cu_4(S_2)(S)_2]^-$ layers, which is also mixed-valent and contains both S_2^{2-} and S^{2-} and $Cu^{1+/2+}$ (or S_2^{2-} and S^- and Cu^+) (Figure 5). Significant differences between the structures of $NaCu_4S_4$ and $NaCu_6Se_4$ are the thickness of the copper chalcogenide layer and the coordination geometry of Cu. Compared to the $NaCu_4S_4$ structure in which one of the two crystallographically independent Cu atoms is tetrahedral and the other one is three-coordinate (trigonal planar), all three distinct Cu atoms in $NaCu_6Se_4$ are tetrahedrally coordinated.

The formal oxidation states of $NaCu_6Se_4$ do not balance unless we invoke selenium mixed-valency. If all monoselenides are considered as −2, then the charges on the metal reduce to $(Na^+)(Cu^+)_5(Cu^{2+})(Se^{2-})_4$. This is unlikely because the coexistence of Cu^{2+} and Se^{2-} tends to be unstable with respect to electron transfer from the highly reducing Se^{2-} anions to the highly oxidizing Cu^{2+} cations. Alternatively, if all copper atoms are considered as +1, then the charges on the monoselenides reduce to $(Na^+)(Cu^+)_6(Se^{1-})(Se^{2-})_3$. If all copper atoms are assigned the +1 oxidation state, then the average oxidation state of Se is −1.75, less than −2 for a filled Se^{2-} p-band. The electron deficiency at Se can be delocalized in the valence band, or localized through a structural distortion as diselenide, or both. In $NaCu_6Se_4$ no Se−Se bonds exist, so the holes can be completely delocalized through the monoselenide p-band. This situation is reminiscent of that found in CuS,[49,50] $NaCu_4S_4$,[14] or $Na_3Cu_4S_4$,[4,17] all known metallic mixed-valence compounds.

Physical Properties. *Charge Transport Properties.* The electrical properties of $NaCu_6Se_4$ were measured on annealed pressed pellets (with 81% of the theoretical density) of a polycrystalline sample. A rectangular piece 3 × 2.5 × 0.8 mm^3 was cut from the annealed pellet and polished. The electrical conductivity of this compound exhibits typical metallic behavior over the temperature range 2−400 K. As shown in Figure 6, the conductivity of $NaCu_6Se_4$ is ∼3000 S/cm at room temperature and increases to 16500 S/cm at 2 K. $NaCu_6Se_4$ possesses a Seebeck coefficient of ∼5 $\mu V\ K^{-1}$ at room temperature, with weak temperature dependence in the region 300−500 K (Figure 7a). A positive Seebeck coefficient suggests that holes are the dominant charge carriers (p-type).

dx.doi.org/10.1021/ic502137m | *Inorg. Chem.* 2014, 53, 12191−12198

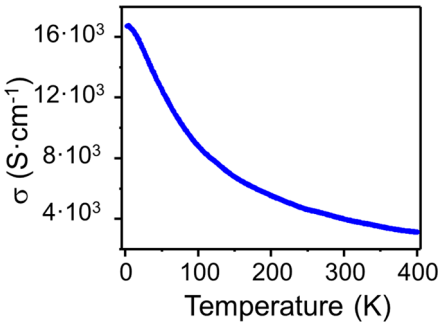

Figure 6. Electrical conductivity data as a function of temperature for an annealed pressed pellet of polycrystalline $NaCu_6Se_4$.

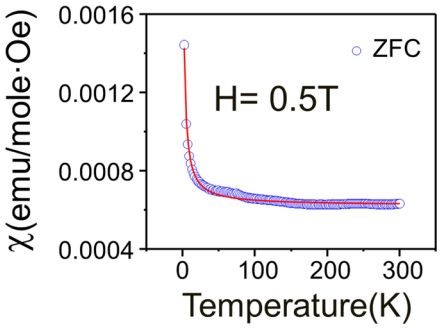

Figure 8. Temperature dependence of the molar magnetic susceptibility for a sample of $NaCu_6Se_4$, measured in an applied field of 5000 Oe.

Hall effect measurements were conducted on annealed pressed pellets of $NaCu_6Se_4$ to determine the concentration and mobility of carriers (Supporting Information Figure S1). In the experiment, ρ_H was taken as $\rho_H = [\rho_{(+H)} - \rho_{(-H)}]/2$ for each point to eliminate any effects from misaligned Hall electrodes. The Hall resistivity, ρ_H, is positive below room temperature, yielding a positive Hall coefficient $R_H = \rho_H/H$, confirming the finding from the Seebeck measurement that holes are indeed the dominant charge carriers in $NaCu_6Se_4$ (Supporting Information Figure S2). The high carrier concentration (Figure 7b) of $p \sim 2.8(3) \times 10^{21}$ cm^{-3} at 300 K is consistent with the formula $NaCu_6Se_4$ which has 0.56 holes per formula unit. The hole mobility, as calculated from the Hall effect and the electrical conductivity data, is approximately 8.75 cm^2/V s at 300 K.

The magnetic susceptibility of polycrystalline $NaCu_6Se_4$, measured at $H = 0.5$ T over the range 2−300 K, is shown in Figure 8. This compound exhibits Pauli paramagnetism with a small temperature-independent contribution of $6.24(5) \times 10^{-4}$ emu/formula unit at $H = 5000$ Oe, Curie constant $C = 0.0028(5)$ emu K/mol, and Weiss constant $\theta = -1.47(2)$ K, as is characteristic of metals. At low temperatures, a paramagnetic tail was observed, as also reported for $Ba_{1-x}K_xCu_2S_2$,[51] KCu_4S_3,[52] $K_2Cu_5Te_5$,[25] $NaBa_2Cu_3S_5$,[13] and $Cs_3Cu_{20}Te_{13}$.[26]

Band Structure Calculations. The electronic band structure of $NaCu_6Se_4$ (Figure 9a) was examined by DFT calculations confirming the metallic character of this mixed valence compound. Both the valence and conduction bands in $NaCu_6Se_4$ show a dispersive character suggesting high electron and hole mobility which was also verified by Hall measurements. Seven bands cross the Fermi level around the Γ and Λ points (directions along the $[Cu_6Se_4]^-$ layers), and the separation of valence and conduction bands becomes maximum at directions normal to the $[Cu_6Se_4]^-$ slabs.

The partial density of states (DOS) plot (Figure 9b) shows that the valence and conduction bands are mainly composed of Cu d-bands and Se p-bands at the Fermi level and up to 12 eV with a comparable contribution of each band to the total DOS. Bands from −7 eV up to near the Fermi level are predominantly Cu d-bands which constitute most of the valence spectra. Se and Na s-bands are located primarily in the −12 to −15 eV range (not shown). Interestingly, a small gap of a few meV is present around 570 meV above the Fermi level. Electronic band structure calculations of the hypothetical isostructural $CaCu_6Se_4$ analogue show that the Fermi level lies in the gapped region (Supporting Information Figures S3 and S4) of the electronic structure, suggesting that the hypothetical analogous $CaCu_6Se_4$ compound is a narrow gap semiconductor.

CONCLUDING REMARKS

The new 2D compound, $NaCu_6Se_4$, forms from the reaction of Na_2Se_x and Cu, as well as by direct combination reactions. The compound has unique $[Cu_6Se_4]^-$ layers sandwiching the Na cations. Despite the incongruent melting of $NaCu_6Se_4$, we were able to grow single crystals by slow-cooling from the melt. After determining the crystal structure for this new ternary compound, we successfully synthesized the material as a single phase via two separate synthesis protocols. Electronic band structure calculations and physical property measurements reveal p-type metallic behavior for $NaCu_6Se_4$, with moderately high electrical conductivity and hole carrier mobilities.

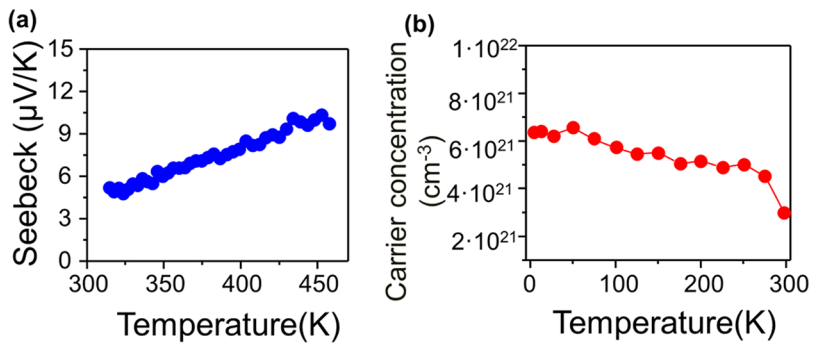

Figure 7. (a) Variable-temperature thermoelectric power data for a polycrystalline sample of $NaCu_6Se_4$ showing p-type behavior. (b) Carrier concentration as a function of temperature for $NaCu_6Se_4$.

dx.doi.org/10.1021/ic502137m | *Inorg. Chem.* 2014, 53, 12191−12198

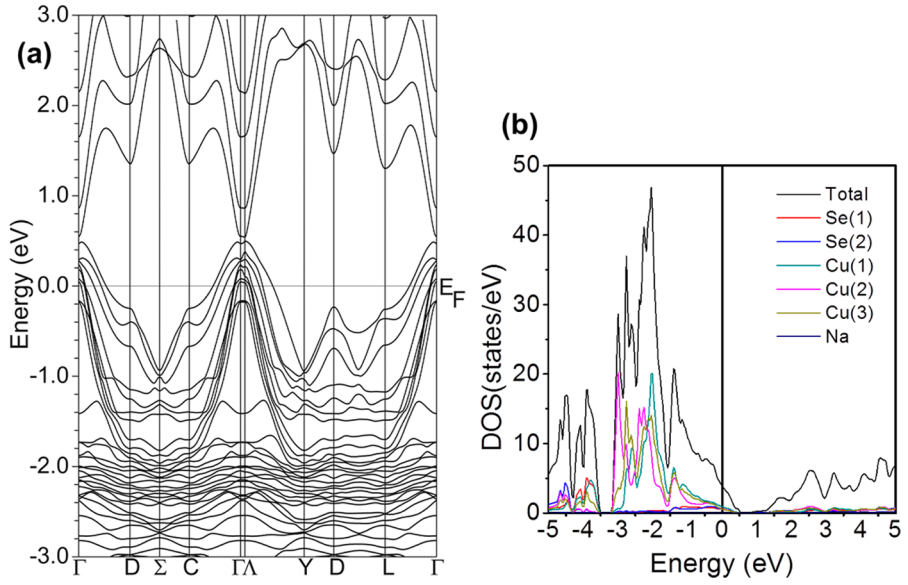

Figure 9. (a) Calculated electronic band structure of $NaCu_6Se_4$. (b) Density of states (DOS) plot near the Fermi level for $NaCu_6Se_4$.

■ ASSOCIATED CONTENT

Supporting Information

Crystallographic data in CIF format. Further details in Figures S1−S4. This material is available free of charge via the Internet at http://pubs.acs.org.

■ AUTHOR INFORMATION

Corresponding Author

*E-mail: m-kanatzidis@northwestern.edu.

Notes

The authors declare no competing financial interest.

■ ACKNOWLEDGMENTS

The work was supported by the U.S. Department of Energy, Office of Science, Materials Sciences and Engineering Division. Use of the Electron Microscopy Center for Materials Research at Argonne National Laboratory was supported by the U.S. Department of Energy, Office of Science, Office of Basic Energy Sciences, under Contract DE-AC02-06CH11357.

■ REFERENCES

(1) Mitchell, K.; Ibers, J. A. *Chem. Rev.* **2002**, *102*, 1929−1952.
(2) Malliakas, C. D.; Kanatzidis, M. G. *J. Am. Chem. Soc.* **2007**, *129*, 10675−10677.
(3) Burschka, C. *Z. Naturforsch., B: Anorg. Chem., Org. Chem.* **1979**, *34*, 396−397.
(4) Peplinski, Z.; Brown, D.; Watt, T.; Hatfield, W.; Day, P. *Inorg. Chem.* **1982**, *21*, 1752−1755.
(5) Vouroutzis, N.; Manolikas, C. *Phys. Status Solidi A* **1989**, *111*, 491−497.
(6) Ohtani, T.; Tachibana, Y.; Ogura, J.; Miyake, T.; Okada, Y.; Yokota, Y. *J. Alloys Compd.* **1998**, *279*, 136−141.
(7) Brown, D. R.; Day, T.; Borup, K. A.; Christensen, S.; Iversen, B. B.; Snyder, G. J. *Appl. Mater.* **2013**, *1*, 052107-1−052107-10.
(8) Bychkov, E. *Solid State Ionics* **2009**, *180*, 510−516.
(9) Liu, H.; Shi, X.; Xu, F.; Zhang, L.; Zhang, W.; Chen, L.; Li, Q.; Uher, C.; Day, T.; Snyder, G. J. *Nat. Mater.* **2012**, *11*, 422−425.
(10) Gabor, A. M.; Tuttle, J. R.; Albin, D. S.; Contreras, M. A.; Noufi, R.; Hermann, A. M. *Appl. Phys. Lett.* **1994**, *65*, 198−200.
(11) Androulakis, J.; Peter, S. C.; Li, H.; Malliakas, C. D.; Peters, J. A.; Liu, Z.; Wessels, B. W.; Song, J.-H.; Jin, H.; Freeman, A. J.; Kanatzidis, M. G. *Adv. Mater.* **2011**, *23*, 4163−4167.
(12) Axtell, E. A.; Park, Y.; Chondroudis, K.; Kanatzidis, M. G. *J. Am. Chem. Soc.* **1998**, *120*, 124−136.
(13) Sturza, M.; Han, F.; Shoemaker, D. P.; Malliakas, C. D.; Chung, D. Y.; Jin, H.; Freeman, A. J.; Kanatzidis, M. G. *Inorg. Chem.* **2013**, *52*, 7210−7217.
(14) Zhang, X.; Kanatzidis, M. G.; Hogan, T.; Kannewurf, C. R. *J. Am. Chem. Soc.* **1996**, *118*, 693−694.
(15) Brown, D. B.; Zubieta, J. A.; Vella, P. A.; Wrobleski, J. T.; Watt, T.; Hatfield, W. E.; Day, P. *Inorg. Chem.* **1980**, *19*, 1945−1950.
(16) Fleming, R. M.; Terhaar, L. W.; Disalvo, F. J. *Phys. Rev. B* **1987**, *35*, 5388−5391.
(17) Burschka, C.; Bronger, W. *Z. Naturforsch., B: Anorg. Chem., Org. Chem.* **1979**, *34B*, 675−677.
(18) Schils, H.; Bronger, W. *Z. Anorg. Allg. Chem.* **1979**, *456*, 187−193.
(19) Zhang, X.; Zhang, X.; Park, Y. B.; Hogan, T.; Schindler, J. L.; Kannewurf, C. R.; Seong, S.; Albright, T.; Kanatzidis, M. G. *J. Am. Chem. Soc.* **1995**, *117*, 10300−10310.
(20) Bronger, W.; Schils, H. *J. Less. Common. Met.* **1982**, *83*, 279−285.
(21) Berger, R.; Vanbruggen, C. F. *J. Less. Common. Met.* **1984**, *99*, 113−123.
(22) Berger, R.; Eriksson, L. *J. Less. Common. Met.* **1990**, *161*, 165−173.
(23) Berger, R.; Meerschaut, A. *Eur. J. Solid State Inorg. Chem.* **1988**, *25*, 279−288.
(24) Emirdag, M.; Schimek, G. L.; Kolis, J. W. *J. Chem. Soc., Dalton Trans.* **1999**, 1531−1532.
(25) Park, Y.; Kanatzidis, M. G.; Kannewurf, C. R.; Degroot, D. C.; Schindler, J. *Angew. Chem., Int. Ed. Engl.* **1991**, *30*, 1325−1328.
(26) Huai, W.-J.; Shen, J.-N.; Lin, H.; Chen, L.; Wu, L.-M. *Inorg. Chem.* **2014**, *53*, 5575−5580.
(27) Park, Y.; Kanatzidis, M. G. *Chem. Mater.* **1991**, *3*, 781−783.
(28) Munson, R. A.; DeSorbo, W.; Kouvel, J. S. *J. Chem. Phys.* **1967**, *47*, 1769−1770.
(29) Meissner, W. *Z. Phys.* **1929**, *58*, 570−571.
(30) Shoenberg, D. *Nature* **1938**, *142*, 874−875.
(31) Stevels, A. L. N.; Jellinek, F. *Recl. Trav. Chim.* **1971**, *90*, 273−283.
(32) Stevels, A. L. N.; Wiegers, G. A. *Recl. Trav. Chim.* **1971**, *90*, 352−359.
(33) Fleming, R. M.; Ter Haar, L. W.; DiSalvo, F. *J. Phys. Rev. B* **1987**, *35*, 5388.
(34) Savelsberg, G.; Schafer, H. *Z. Naturforsch., B: J. Chem. Sci.* **1978**, *33*, 370−373.

(35) *X-AREA; X-SHAPE; X-RED*; STOE & Cie GmbH: Darmstadt, Germany, 2004.
(36) Sheldrick, G. M. *Acta Crystallogr., Sect. A: Found. Crystallogr.* **2008**, *64*, 112−122.
(37) Petricek, V.; Dusek, M.; Palatinus, L. *Jana2006, The Crystallographic Computing System*; Institute of Physics: Praha, Czech Republic, 2006.
(38) Carvajal, R. *J. Phys. Rev. B* **1993**, *192*, 55−69.
(39) Wood, C.; Chmielewski, A.; Zoltan, D. *Rev. Sci. Instrum.* **1988**, *59*, 951−954.
(40) Singh, D. *Planewaves, Pseudopotentials, and the LAPW Method*; Kluwer Academic: Boston, MA, 1994.
(41) Kohn, W.; Sham, L. J. *Phys. Rev. B* **1965**, *140*, 1133−1138.
(42) Hohenberg, P.; Kohn, W. *Phys. Rev. B* **1964**, *136*, 864−871.
(43) Perdew, J. P.; Burke, K.; Ernzerhof, M. *Phys.Rev. Lett.* **1996**, *77*, 3865−3868.
(44) Koelling, D. D.; Harmon, B. N. *J. Phys. C* **1977**, *10*, 3107−3114.
(45) Blaha, P.; Schwarz, K.; Madsen, G.; Kvasnicka, D.; Luitz, J.; Schwarz, K. *WIEN2k*; Technische Universität Wien: Vienna, 2001.
(46) Heyding, R. D.; Murray, R. M. *Can. J. Chem.* **1976**, *54*, 841−848.
(47) Taylor, C. A.; Underwood, F. A. *Acta Crystallogr.* **1960**, *13*, 361−362.
(48) Morimoto, N.; Koto, K. *Science* **1966**, *152*, 345−345.
(49) Takeuchi, K.; Kudoh, Y.; Sato, G. *Z. Kristallogr.* **1985**, *173*, 119−128.
(50) Fjellvag, H.; Gronvold, F.; Stolen, S. *Z. Kristallogr.* **1988**, *184*, 111−121.
(51) Zhang, X.; Hogan, T.; Kannewurf, C. R.; Kanatzidis, M. G. *J. Alloys Compd.* **1996**, *236*, 1−5.
(52) Schramm, C. J.; Scaringe, R. P.; Stojakovic, D. R.; Hoffman, B. M.; Ibers, J. A.; Marks, T. J. *J. Am. Chem. Soc.* **1980**, *102*, 6702−6713.